Proceedings 10th NUMGE 2023
10th European Conference on Numerical Methods in Geotechnical Engineering
Zdravkovic L, Kontoe S, Taborda DMG, Tsiampousi A (eds)

https://doi.org/10.53243/NUMGE2023-115

Temperature-dependent residual shear strength of bentonite: experimental investigation and numerical modelling

S. Tourchi, M. Loche, G. Scaringi

Institute of Hydrogeology, Engineering Geology and Applied Geophysics, Faculty of Science, Charles University, Prague, Czech Republic.

ABSTRACT: This paper describes experimental and numerical approaches to account for the effect of temperature on the residual shear strength of soil under slow-to-rapid shearing rates. We used ring-shear test results obtained on reconstituted samples of Ca-Mg bentonite, which were sheared to evaluate the drained residual friction angle (φ'_{res}) under various confining stresses ($\sigma'_v = 50 - 150\ kPa$), shearing rates ($v = 0.018 - 44.5\ mm/min$), and temperatures ($T = 20 - 55\ °C$). These results highlighted a dependence of φ'_r on both v and T. In particular, thermal strengthening was observed under relatively low v, which turned into thermal weakening under high v. To reproduce this behaviour, we propose a non-isothermal viscoplastic model, which we implemented in a finite-element computer code for thermo-hydro-mechanical analysis of porous media. We calibrated the model using the experimental results, achieving a satisfactory performance. Owing to the significance of thermal effects in soil, we argue that approaches such as ours should be developed further and incorporated in modelling practices.

Keywords: Residual shear strength; thermo-hydro-mechanical coupling; thermal weakening; bentonite.

1 INTRODUCTION

A striking feature of landslides in over-consolidated clays is the localisation of deformation into thin shear bands, often assimilated to *slip surfaces*. Slip-surface soils in reactivated landslides are often clay-enriched and offer little shear resistance owing to the smoothing and particle alignment caused by the large shearing strains attained. Knowledge of this minimal resistance, the *residual shear strength* (τ_{res}), is crucial for investigating landslide mechanisms and evaluating the reactivation potential (Mesri and Shahien, 2003). Many researchers have soil behaviours under shearing and pointed out that τ_r is influenced by several factors, including the mineral composition, pore fluid composition, rate of shearing (v), and grain shape (Scaringi and Di Maio, 2016). Owing to the importance of this parameter in geotechnical practice, relationships between τ_{res} (or the residual friction coefficient, $\mu_{res} = \tau_{res}/\sigma'_v$, where σ'_v is the normal effective stress, or the residual friction angle φ'_{res}, remembering that $\mu_{res} = \tan\varphi'_{res}$) and basic soil characteristics, such as the clay fraction and index properties, have been sought (Collotta et al., 1989; Wesley, 2003; Roháč et al., 2019).

Under a given confining stress σ_v, the available resistance along a slip surface decreases as the pore water pressure u increases (reflecting a decrease in σ'_v), which promotes slope instability (Skempton, 1985). Studies highlighted that changes in ground temperature, which can be significant at slip-surface depths especially for shallow landslides, also can alter the available resistance. While this is well known in seasonally-frozen soils, it is much less studied in ground temperature ranges typical of temperate and warm climates (Shibasaki et al., 2016; Scaringi and Loche, 2022; Scaringi et al., 2022; Loche and Scaringi, 2023). In fact, most studies investigating thermal effects have done so while focusing on the peak or critical-state strengths, while the role of temperature on the residual shear strength remains poorly understood (Shibasaki et al. 2017).

In this study, we made use of recent experimental results obtained on a commercial Ca-Mg-bentonite under σ'_v and v values typical of slow-to-rapid landslides, and temperatures T in the range of $20 - 55\ °C$ (Loche and Scaringi, 2023b). The results were interpreted by proposing a non-isothermal constitutive law, which considers the effect of temperature on the stiffness and strength parameters and the thermal softening of the slip surface.

2 TEMPERATURE-CONTROLLED RING SHEAR TESTS

A commercially available bentonite was employed for temperature-controlled ring-shear tests. The material, known as the *Czech B75 Bentonite*, is a Ca-Mg-bentonite extracted from a deposit in Černý vrch, Czech Republic. Some of the soil properties are listed in Table 1. Further characterisation can be found in (Sun et al., 2020).

Table 1. Basic properties of the tested bentonite.

Parameter	Value	Parameter	Value
Specific gravity, G_s	2.87	Activity, *A*	2.7
Liquid limit, *LL*	217	clay fraction, *c.f.*	61
Plastic limit, *PL*	51	silt fraction, *s.f.*	33
Ca-Mg montmorillonite	85	USCS name	CH

The tests were performed in a conventional Bromhead-type ring-shear apparatus (Bromhead, 1979) equipped with a temperature-change device allowing water circulation in a closed circuit between an external temperature-controlled bath and the shear-box bath. The device accommodates a 5 mm-thick annular sample sandwiched between brass porous platens that are roughened to avoid interface shearing. Lateral friction was minimised by ensuring post-consolidation sample thicknesses larger than 4.25 mm. The available range of shear rates was exploited ($v = 0.018 - 44.5\ mm/min$), which are associated with slow-to-rapid landslide movements. The samples were reconstituted following Burland (1990) and consolidated stepwise to $\sigma'_v = 600\ kPa$. They were then unloaded to $\sigma'_v = 50 - 150\ kPa$ before shearing. Under each σ'_v level, v was increased stepwise. A schematic illustration of the test specimen is shown in Figure 1. Further details can be found in Loche and Scaringi (2023b).

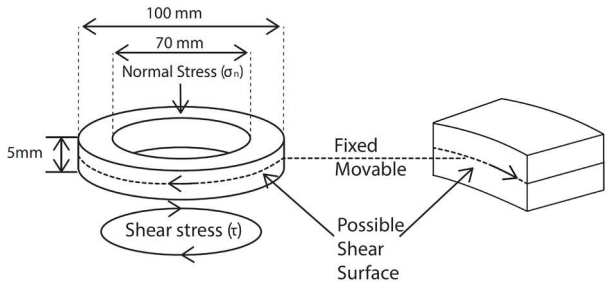

Figure 1. Schematic illustration of the test specimen during a ring-shear experiment.

3 TEST PROCEDURE AND RESULTS

Following the path shown in Figure 2, heating-cooling tests were conducted. After attaining the residual shear strength under the chosen stress and displacement rate conditions at room temperature (20 °C), the bath temperature was increased to 55 °C and was kept constant over a sufficient shearing distance before gradually decreasing it back to the initial value. The results of these tests are shown in Figure 3 in terms of μ_{res}.

Under slow shearing (0.018 mm/min), μ_{res} increased as T increased (Figure 3a and 3b). However, this behaviour was not observed under moderate shearing rate (1.78 mm/min) (Figure 3e and 3f), where some thermal weakening was observed. Interestingly, weak or negligible strength change was seen for the tests at v = 0.5 mm/min (Figure 3c and 3d), which seems an upper threshold for thermal strengthening and roughly corresponds (if size-independent) to moderate landslide velocities. Results under high shearing rates (44.5 mm/min) are not shown for brevity. Furthermore, ensuring drained shearing under such rates may have been challenging.

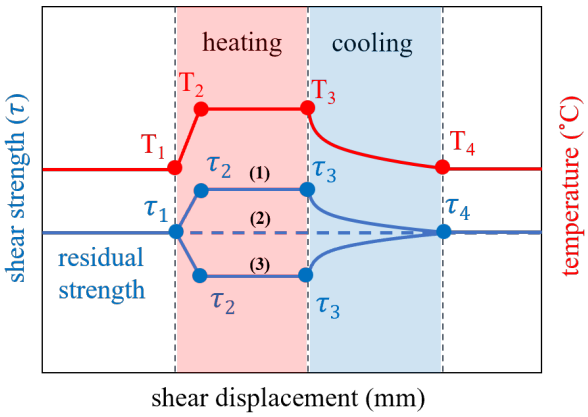

Figure 2. Schematic illustration of temperature-controlled (heating-cooling) tests.

A summary of the results is shown in Figure 4, which shows the failure envelopes obtained at 0.018 mm/min, 0.5 mm/min, and 1.78 mm/min, respectively. At the lowest rate, an increase in μ_{res} by about 13% was evaluated (from ~0.15 to ~0.17). At the threshold rate, μ_{res} remained practically constant (-2%, from ~0.22 to ~0.21), and at the moderate rate, a 46% decrease was evaluated (from ~0.28 to ~0.15).

4 THEORETICAL FORMULATION

4.1 Non-isothermal elasto- viscoplastic model for the slip surface

An elasto-viscoplastic formulation is proposed to model the mechanical response of slip surfaces (or thin shear bands). We take as our starting point an observation of what happens when overconsolidated bentonite samples are tested in a ring-shear box, as illustrated schematically in Figure 1. This observation prompts us to propose a non-isothermal model of slip surface strength degradation in which relative shear displacements can occur in concentrated shear bands with temperature elevation.

The assumed model of a shear band in soil has much in common with cohesive force models of tensile cracks. In particular, we follow the development by Zandarin et al. (2013) for interface rock joint elements. Herein, we consider the shear band simply as a surface of discontinuity on which there exists a definite relation between shear stress and relative displacement.

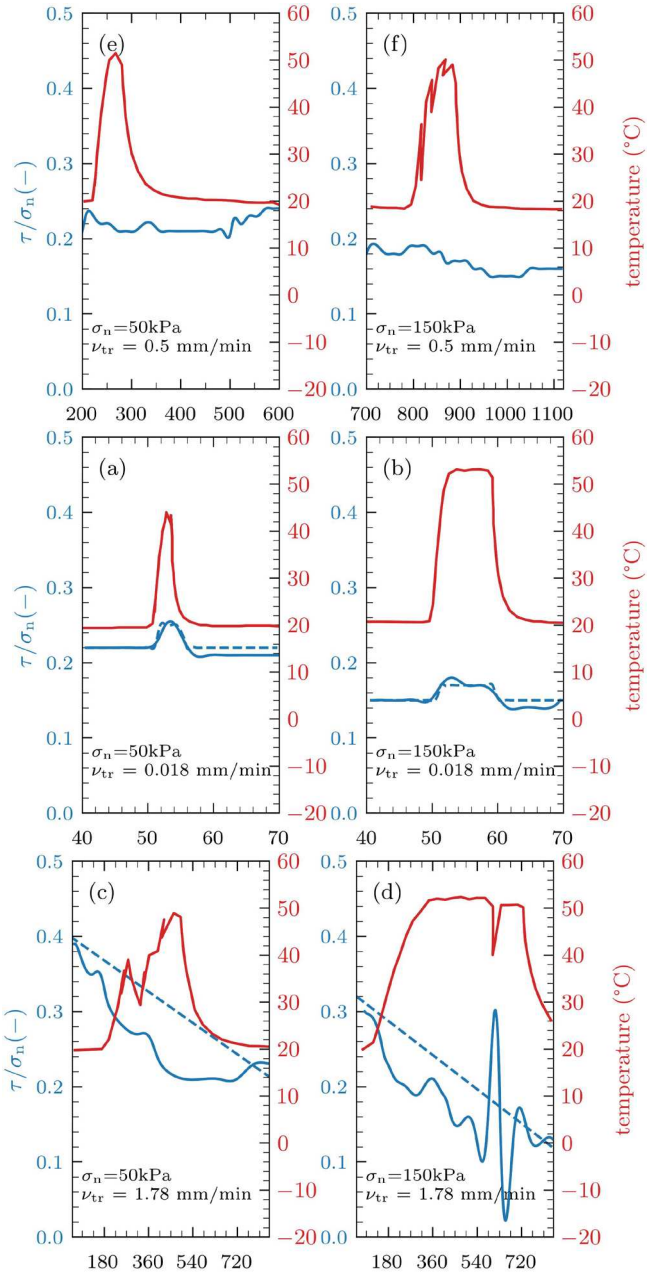

Figure 3. Comparison between shear resistance and temperature during heating-cooling ring-shear tests on bentonite (dashed lines represent model result).

The elastic formulation describes the normal and tangential elastic stiffnesses by means of a nonlinear law which depends on the slip surface thickness and temperature change. The viscoplastic formulation allows the treatment of non-associated plasticity and thermomechanical softening behaviour of slip surfaces subjected to shear displacements.

Total displacements ($\boldsymbol{w}$) are calculated by adding reversible elastic displacements ($\boldsymbol{w}^{\mathrm{e}}$), and viscoplastic displacements ($\boldsymbol{w}^{\mathrm{vp}}$), which are zero when stresses are below a threshold value (the yield surface):

$$\boldsymbol{w} = \boldsymbol{w}^{\mathrm{e}} + \boldsymbol{w}^{\mathrm{vp}} \tag{1}$$

A two-element vector represents normal and shear (relative) displacements in the two-dimensional case:

$$\boldsymbol{w^T} = [\boldsymbol{u_n}, \boldsymbol{u_s}] \tag{2}$$

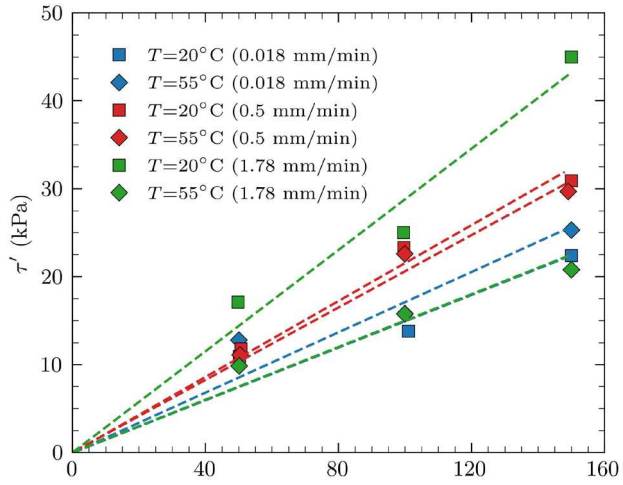

Figure 4. Residual shear strength envelopes at T = 20 °C and 55 °C for the tested bentonite v = 0.018 mm/min and 0.5 and 1.78 mm/min shear rates.

4.2 *Elastic behaviour*

The elastic behaviour of the slip surface relates stresses (σ' and τ) to displacements (u_{n} and u_{s}) through the normal (K_{n}) and tangential stiffness (K_{s}), respectively. The normal stiffness depends on the thickness of the slip surface, as follows:

$$\begin{Bmatrix} u_{\mathrm{n}} \\ u_{\mathrm{s}} \end{Bmatrix} = \begin{bmatrix} 1/K_{\mathrm{n}} & 0 \\ 0 & 1/K_{\mathrm{s}} \end{bmatrix} \begin{Bmatrix} \sigma' \\ \tau \end{Bmatrix} \tag{3}$$

$$K_n(T_0) = \frac{m}{t - t_{\mathrm{min}}} \tag{4}$$

where m is a parameter of the model; t is the thickness of the slip surface and t_{min} is the minimum slip surface tickness.

4.3 *Viscoplastic behaviour*

The viscoplastic formulation consist of a yield surface, a plastic potential, and a softening law. Viscoplastic displacements occur when the stress state of the interface elements reaches a yielding condition. Herein, a hyperbolic yield surface based on Gens et al. (1990) was adopted:

$$F = \tau^2 - (c' - \sigma' \tan\varphi')^2 + (c' - \chi \tan\varphi')^2 \tag{5}$$

where τ is the shear stress, c' is the effective cohesion; σ' is the effective normal stress, $\tan\varphi'$ is the tangent of the effective angle of internal friction and χ is a model parameter.

4.4 *Softening law*

The strain-softening of the slip-surface soil under shear stress is modelled by means of the degradation of the

strength parameters, which depends linearly on viscoplastic relative shear displacements. The cohesion decays from the initial value to zero and the friction angle decays from the peak to the residual value as a function of a critical viscoplastic shear displacement. Two different values of u^* are used to define the decrease of cohesion (u_c^*) and friction angle $\left(u_{\tan\varphi'}^*\right)$. The mathematical expression is:

$$c' = c_0'\left(1 - \frac{u_{\mathrm{s}}^{\mathrm{vp}}}{u_{\mathrm{c}}^*}\right) \tag{6}$$

where c' is the effective cohesion which corresponds to the viscoplastic shear displacement $u_{\mathrm{s}}^{\mathrm{vp}}$, c_0' is the initial value of effective cohesion, and u_c^* is the critical value of shear displacement, for which the value of c' is zero. Also,

$$\tan\varphi' = \tan\varphi_0' - (\tan\varphi_0' - \tan\varphi_{\mathrm{res}}')\frac{u_{\mathrm{s}}^{\mathrm{vp}}}{u_{\varphi}^*} \tag{7}$$

where $\tan\varphi'$ corresponds to the viscoplastic shear displacement $u_{\mathrm{s}}^{\mathrm{vp}}$, $\tan\varphi_0'$ is the tangent of the peak friction angle, $\tan\varphi_{\mathrm{res}}'$ is the tangent of the internal friction effective residual angle, and u_{φ}^* is the critical value of shear displacement when the value of $\tan\varphi'$ is equal to $\tan\varphi_{\mathrm{res}}'$.

4.4.1 *Viscoplastic displacements*

If $F < 0$, the stress state of the interface element is inside the elastic region; if $F \geq 0$, the displacement is:

$$\frac{\mathrm{d}\dot{\boldsymbol{w}}^{\mathrm{vp}}}{\mathrm{d}t} = \Gamma < \phi\left(\frac{F}{F_0}\right) > \frac{\partial G}{\partial \sigma} \tag{8}$$

where G is a plastic potential, and Γ is a viscosity parameter. In order to ensure that there is no viscoplastic flow inside the yield locus, the following consistency conditions should be met:

$$\left.\begin{array}{l} < \phi\left(\frac{F}{F_0}\right) \geq 0 \ (\ if\ F < 0) \\ < \phi\left(\frac{F}{F_0}\right) \geq \phi(F) \ (\ if\ F \geq 0) \end{array}\right\} \tag{9}$$

where F_0 can be any convenient value of F to render the above expressions non-dimensional. In this study $F_0 = 1$. The normal and shear viscoplastic displacement rates, $\boldsymbol{u}_{\mathrm{n}}^{\mathrm{vp}}$ and $\boldsymbol{u}_{\mathrm{s}}^{\mathrm{vp}}$, are given by power laws:

$$\Delta\dot{\boldsymbol{u}}_{\mathrm{n}}^{\mathrm{vp}} = \Gamma F^N \frac{\partial G}{\partial \sigma} \tag{10}$$

$$\Delta\dot{\boldsymbol{u}}_{\mathrm{s}}^{\mathrm{vp}} = \Gamma F^N \frac{\partial G}{\partial \tau} \tag{11}$$

where N is the exponent of the power law.

4.5 *Plastic potential and dilatancy*

The associated rule allows the calculation of displacements directions. The derivative of G with respect to stresses includes the parameters $f_{\sigma}^{\mathrm{dil}}$ and f_c^{dil}, which take into account the dilatant behaviour of the slip surface under shear stresses (Garello, 1999):

$$\frac{\partial G}{\partial \boldsymbol{\sigma}} = \left[2\tan\phi'(c' - \sigma'\tan\phi')f_{\sigma}^{dil}f_c^{dil}, 2\tau\right]^T \tag{12}$$

where $f_{\sigma}^{\mathrm{dil}}$ accounts for the decrease of dilatancy with the level of the normal stress acting on the interface, and f_c^{dil} defines the degradation of the interface surfaces due to shear displacements. Note that the superscript T indicates the transpose and the quantity in [] is a vector. The following expressions describe these effects:

$$f_{\sigma}^{\mathrm{dil}} = \left(1 - \frac{|\sigma'|}{q_{\mathrm{u}}}\right)\exp\left(-\beta_{\mathrm{d}}\frac{|\sigma'|}{q_{\mathrm{u}}}\right) \tag{13}$$

$$f_c^{\mathrm{dil}} = \frac{c'}{c_0'} \tag{14}$$

where q_{u} is the compression strength of the material for which dilatancy vanishes, β_{d} is a model parameter, and c' is the cohesion value for the viscoplastic shear displacement $u_{\mathrm{s}}^{\mathrm{vp}}$.

4.6 *Non-isothermal formulation*

4.6.1 *Thermoelastic components*

Preliminary data suggest that the elastic domain varies with temperature. Thus, the normal and tangential stiffness are assumed to be a function not only of viscoplastic shear displacements but also of temperature:

$$K_n(T) = \begin{cases} K_n(T_0)[1 + \mu_K\ln(T/T_0)] & \dot{\boldsymbol{u}}_{\mathrm{n}}^{\mathrm{vp}} < (\dot{\boldsymbol{u}}_{\mathrm{n}}^{\mathrm{vp}})_{tr} \\ K_n(T_0) & \dot{\boldsymbol{u}}_{\mathrm{n}}^{\mathrm{vp}} = (\dot{\boldsymbol{u}}_{\mathrm{n}}^{\mathrm{vp}})_{tr} \\ K_n(T_0)[1 - \mu_K\ln(T/T_0)] & \dot{\boldsymbol{u}}_{\mathrm{n}}^{\mathrm{vp}} > (\dot{\boldsymbol{u}}_{\mathrm{n}}^{\mathrm{vp}})_{tr} \end{cases} \tag{15}$$

where $K_n(T_0)$ and $K_n(T)$ are normal stiffness at reference and a given temperature, respectively, μ_K controls the rate of variation of normal stiffness with temperature, and $v\ and\ v_{tr}$ are the shearing rate and threshold shearing rate, respectivly. The tangential stiffness varies with temperature with a logarithmic relationship similar to Equation (14):

$$K_s(T) = \begin{cases} K_s(T_0)[1 + \mu_s\ln(T/T_0)] & \dot{\boldsymbol{u}}_{\mathrm{s}}^{\mathrm{vp}} < (\dot{\boldsymbol{u}}_{\mathrm{s}}^{\mathrm{vp}})_{tr} \\ K_s(T_0) & \dot{\boldsymbol{u}}_{\mathrm{s}}^{\mathrm{vp}} = (\dot{\boldsymbol{u}}_{\mathrm{s}}^{\mathrm{vp}})_{tr} \\ K_s(T_0)[1 - \mu_s\ln(T/T_0)] & \dot{\boldsymbol{u}}_{\mathrm{s}}^{\mathrm{vp}} > (\dot{\boldsymbol{u}}_{\mathrm{s}}^{\mathrm{vp}})_{tr} \end{cases} \tag{16}$$

where $K_s(T_0)$ and $K_s(T)$ are tangential stiffness at reference and a given temperature, respectively and μ_S controls the rate of variation of normal stiffness with temperature.

4.6.2 Thermoplastic components

In the context of landslides, key thermal effects in clays are those that lead to irreversible plastic deformations and, therefore, those affecting the failure of slip surfaces. As discussed in Section 3, the residual shear strength of the tested bentonite is temperature-dependent. This implies that larger plastic deformations and a failure surface can be expected under higher temperatures, such as those possibly induced by near-surface ground temperature changes. Following (Tourchi et al., 2020; Tourchi et al., 2022), this behaviour can be incorporated by assuming that the strength parameters also depend on temperature.

A hyperbolic Mohr-Coulomb-type yield function characterises the adopted model; therefore, the dependence of strength on temperature can also be incorporated through the parameters ϕ and c (Tourchi, 2020). However, since no cohesion was observed in the experiment (which is comprehensible in the residual condition), only the mobilised friction angle must be a function of temperature. As such, Equation (16) can be adopted to define ϕ_{res} as a function of temperature in the following way:

$$\varphi_{\text{res}}^{T} = \begin{cases} \varphi_{\text{res}}^{T_0}\left[1+\mu_{\varphi}\ln(T/T_0)\right] & \dot{\boldsymbol{u}}_{\text{s}}^{\text{vp}} < (\dot{\boldsymbol{u}}_{\text{s}}^{\text{vp}})_{tr} \\ \varphi_{\text{res}}^{T_0} & \dot{\boldsymbol{u}}_{\text{s}}^{\text{vp}} = (\dot{\boldsymbol{u}}_{\text{s}}^{\text{vp}})_{tr} \\ \varphi_{\text{res}}^{T_0}\left[1-\mu_{\varphi}\ln(T/T_0)\right] & \dot{\boldsymbol{u}}_{\text{s}}^{\text{vp}} > (\dot{\boldsymbol{u}}_{\text{s}}^{\text{vp}})_{tr} \end{cases} \quad (17)$$

where $\varphi_{res}^{T_0}$ and φ_{res}^{T} are the residual friction angle at the reference temperature (T_0) and elevated temperature (T), and coefficient μ_{φ} is a model parameter that controls the thermal evolution of the friction angle.

The incorporated dependence of the yield function with temperature requires the modification of the standard form of Prager's consistency condition. In the case of plastic loading, the latter reads:

$$dF = \frac{\partial F}{\partial \sigma} d\sigma + \frac{\partial F}{\partial \varphi_{\text{mob}}} d\varphi_{\text{mob}} = 0 \quad (18)$$

where

$$d\varphi = \frac{\partial \varphi}{\partial u_s^{vp}}\, du_s^{vp} + \frac{\partial \varphi}{\partial T} dT \quad (19)$$

Therefore, plastic deformations also are affected by the thermal dependence of the strength parameters.

5 NUMERICAL SIMULATION OF RING-SHEAR TEST

The ring shear tests with rates of 0.018 mm/min and 1.78 mm/min were selected to check the capabilities of the proposed model. The numerical simulation was carried out with the finite-element code Code_Bright (Olivella et al. 1996) employing the interface element (Carol et al., 1997) and the new non-isothermal constitutive law proposed above.

The simulation is assumed under axisymmetric two-dimensional coupled THM conditions. The dimensions of the model are $120\ \text{mm} \times 60\ \text{mm}$. The rate of displacements used in the test is applied on movable part. Fixed part is horizontally fixed and it is vertically fixed at the bottom. The net normal stresses used in the test are applied on the top of movable part. The interface element is discretized using 10 elements. An initial constant temperature of $21{,}8\ ^{\circ}\text{C}$ has been assumed throughout the geometry. Heat power was applied as a thermal flux on the interface. The fixed and movable parts (Figure 1) are simulated as an elastic material, and the sample is modelled as a visco-plastic zero-thickness element. The parameters are listed in Table 2. The predictions of the numerical analysis are plotted in a dashed line alongside test measurements in Figure 3. The results demonstrate that the material's strength behavior varies significantly with the shearing rate. At slow rates, an increase in strength was observed with temperature, while moderate rates caused weakening. Interestingly, negligible changes were seen at an intermediate rate, suggesting an upper limit for thermal strengthening. The numerical analysis has simulated the various phases of the experiment, as listed in Figure 2. It is apparent that the overall shear behaviour is reasonably well captured by the model for the three loading steps as defined above, and the calculated results are in good agreement with the measured values.

Table 2. Parameters for ring shear samples (elasto visco-plastic model).

Parameter	Value	Unit
Mechanical properties		
Initial normal stiffness parameter, m	60×10^3	kPa
Tangential stiffness, $\boldsymbol{K_s(T_0)}$	166×10^3	kPa/m
Initial friction angle, $\boldsymbol{\varphi_0}$	35	(°)
Residual friction angle, $\boldsymbol{\varphi_{res}^{T_0}}$	8.69 12.18 16	(°)
Initial shear surface thickness, t_0	0.1	mm
Minimum shear surface thickness, t_{min}	0.01	mm
Viscosity, $\boldsymbol{\Gamma}$	1×10^{-2}	s^{-1}
Stress power, N	2.0	-
Critical displacement for cohesion, $\boldsymbol{u_c^*}$	1	mm
Critical displacement for, $\boldsymbol{\tan\varphi}$	1	mm
Uniaxial compressive strength, q_u	600	kPa
Model parameter, $\boldsymbol{\beta_d}$	100	-
Non-isothermal parameters		
Residual friction angle, $\boldsymbol{\varphi_{res}^{T}}$	9.85 11.69 8.53	(°) (°) (°)
Model parameter, $\boldsymbol{\mu_{\varphi}}$	0.5	-

6 CONCLUSIONS

The influence of temperature and shearing rate on the residual shear strength of soils is an important issue in landslides and has been receiving increasing attention. We performed ring-shear test results on a Ca-Mg-bentonite, which showed a significant (and shear rate-dependent) effect of temperature on the residual shear strength, to develop novel mathematical expressions for the strength parameters and normal and tangential stiffnesses of the asymptote of the hyperbolic yield surface. These expressions were introduced as a constitutive law of the interface element implemented in the computer code Code_Bright to simulate the change in residual shear strength with temperature. The experimental features of the tested bentonite samples could be satisfactorily explained by the numerical simulation. Further research is warranted to explore and describe temperature effects under different shearing rates, temperatures, and confining stresses in other clay and non-clay soils, which could prove useful in the assessment of landslide reactivations and runout.

7 ACKNOWLEDGEMENTS

Dr. Tourchi was funded by a Marie Curie MSCA-IF postdoctoral fellowship. Dr. Loche was funded by the GAUK (Project No. 337121). Dr. Scaringi was funded by the GAČR (Project No. 20-28853Y) and the Fund for Intl. Mobil. of researchers at Charles Univ. (MSCA-IF IV; Project No. CZ.02.2.69/0.0/0.0/20_079/0017987).

8 REFERENCES

Bromhead, E.N. 1979. A SIMPLE RING SHEAR APPARATUS. *GROUND ENGINEERING*. **12**(5).

Bucher, F. 1975. *Die Restscherfestigkeit natürlicher Böden, ihre Einflussgrössen und Beziehungen als Ergebnis experimenteller Untersuchungen*. PhD Thesis, ETH Zurich.

Burland, J.B. 1990. On the compressibility and shear strength of natural clays. *Géotechnique*. **40**(3), pp.329–378.

Carol, I., Prat, P.C. and López, C.M. 1997. Normal/Shear Cracking Model: Application to Discrete Crack Analysis. *Journal of Engineering Mechanics*. **123**(8), pp.765–773.

Collotta, T., Cantoni, R., Pavesi, U., Ruberl, E. and Moretti, P.C. 1989. A correlation between residual friction angle, gradation and the index properties of cohesive soils. *Géotechnique*. **39**(2), pp.343–346.

Garello, C.M.L. 1999. *Análisis microestructural de la fractura del hormigón utilizando elementos finitos tipo junta. Aplicación a diferentes hormigones*. PhD Thesis, Universitat Politècnica de Catalunya (UPC).

Loche, M. and Scaringi, G. 2023. Temperature continuously controls the stability of clay slopes.

Mesri, G. and Shahien, M. 2003. Residual shear strength mobilized in first-time slope failures. *Journal of geotechnical and geoenvironmental engineering*. **129**(1), pp.12–31.

Olivella, S., Gens, A., Carrera, J. and Alonso, E.E. 1996. Numerical formulation for a simulator (CODE_BRIGHT) for the coupled analysis of saline media. *Engineering computations*. **13**(7), pp.87–112.

Roháč, J., Scaringi, G., Boháč, J., Kycl, P. and Najser, J. 2019. Revisiting strength concepts and correlations with soil index properties: insights from the Dobkovičky landslide in Czech Republic. *Landslides*. **17**.

Roháč, J., Scaringi, G., Boháč, J., Kycl, P. and Najser, J. 2020. Revisiting strength concepts and correlations with soil index properties: insights from the Dobkovičky landslide in Czech Republic. *Landslides*. **17**(3), pp.597–614.

Scaringi, G. and Di Maio, C. 2016. Influence of Displacement Rate on Residual Shear Strength of Clays. *Procedia Earth and Planetary Science*. **16**, pp.137–145.

Scaringi, G. and Loche, M. 2022. A thermo-hydro-mechanical approach to soil slope stability under climate change. *Geomorphology*. **401**, p.108108.

Scaringi, G., Loche, M., Tourchi, S. and Lombardo, L. 2022. Temperature and slope stability in temperate climate *In*: *17th Plinius Conference on Mediterranean Risks* [Online]. Rome, Italy: Copernicus Meetings. [Accessed 24 January 2023]. Available from: https://meetingorganizer.copernicus.org/Plinius17/Plinius17-26.html.

Shibasaki, T., Matsuura, S. and Hasegawa, Y. 2017. Temperature-dependent residual shear strength characteristics of smectite-bearing landslide soils. *Journal of Geophysical Research: Solid Earth*. **122**(2), pp.1449–1469.

Shibasaki, T., Matsuura, S. and Okamoto, T. 2016. Experimental evidence for shallow, slow-moving landslides activated by a decrease in ground temperature. *Geophysical Research Letters*. **43**(13), pp.6975–6984.

Shibasaki, T. and Yamasaki, T. 2010. Experimental investigation on temperature effect on residual strength characteristics of soils. *Journal of the Japan Landslide Society*. **47**(5), pp.255–264.

Skempton, A.W. 1985. Residual strength of clays in landslides, folded strata and the laboratory. *Géotechnique*. **35**(1), pp.3–18.

Tourchi, S. 2020. *THM analysis of argillaceous rocks with application to nuclear waste underground storage*.[Online] Doctoral thesis, Universitat Politècnica de Catalunya. [Accessed 28 December 2022]. Available from: https://upcommons.upc.edu/handle/2117/340978.

Tourchi, S., Gens, A., Vaunat, J., Mánica, M. and Scaringi, G. 2020. A thermomechanical model for argillaceous rocks J. S. McCartney & I. Tomac, eds. *E3S Web of Conferences*. **205**, p.13014.

Tourchi, S., Malcom, M.A.M., Vaunat, J. and Gens, A. 2022. A thermomechanical model for argillaceous hard soils - weak rocks: application to THM simulation of deep excavations in claystone. *EarthArXiv*.

Wesley, L.D. 2003. Residual strength of clays and correlations using Atterberg limits. *Geotechnique*. **53**(7), pp.669–672.

Zandarin, M.T., Alonso, E. and Olivella, S. 2013. A constitutive law for rock joints considering the effects of suction and roughness on strength parameters. *International Journal of Rock Mechanics and Mining Sciences*. **60**, pp.333–344.